Paper ID APEN-MIT-2021_124
Applied Energy Symposium: MIT A+B
August 11-13, 2021 • Cambridge, USA

Numerical study of indirect evaporative cooler using porous media with dynamic time-independent performance prediction

Wenchao Shi
Department of Building Services Engineering
The Hong Kong Polytechnic University
Hong Kong, China
wenchao511.shi@connect.polyu.hk

Yunran Min
Department of Building Services Engineering
The Hong Kong Polytechnic University
Hong Kong, China
yunran.min@connect.polyu.hk

Hongxing Yang*
Department of Building Services Engineering
The Hong Kong Polytechnic University
Hong Kong, China
hong-xing.yang@polyu.edu.hk

Yi Chen
School of Mechanical and Energy Engineering
Jimei University
Fujian, China
chenyi0511@jmu.edu.cn

Abstract

Air conditioning systems consume a large amount of energy with the rising living standard of human beings. Indirect evaporative cooler, which is increasingly recognized as a promising alternative to partially substitute conventional air-conditioning devices, has been studied extensively to improve the cooling efficiency and save energy in buildings.

Using porous media in the indirect evaporative heat exchangers is a critical approach for performance enhancement. This paper established a two-dimensional plate-type counterflow indirect evaporative cooler model with porous media on the secondary air channel surface. On the one hand, the porous structure was incorporated in the model to alter the boundary layer and flow status. On the other hand, the water retention ability of porous media that potentially improves the surface wettability has been proven to enable the intermittent operation of the water pump. The influence of various porous parameters, i.e. porosity and pore diameter, on the time-independent dynamic variation of the outlet primary air temperature have been quantitatively analyzed. This study provided a theoretical foundation for the studies of the porous plate-type indirect evaporative cooling technology.

Keywords

Air conditioning, Indirect evaporative cooler, porous media, intermittent water spraying, dynamic performance prediction

I. INTRODUCTION

The building energy consumptions have increased promptly due to global climate change and the improvement of people's living standards [1]. In Hong Kong, according to the annual report of energy end-use data from the Electrical and Mechanical Services Department, the energy consumption of air conditioning (AC) accounts for 32% of the total electricity use, which has increased by 16.6% in the past decade [2]. To alleviate the excessive electricity usage, energy-efficient and eco-friendly AC systems received growing research interests. Indirect evaporative cooler (IEC), with high Coefficient of Performance (COP) and low carbon-dioxide emission, is considered as one of the promising approaches to substituting the conventional AC system [3].

In recent years, plate-type IEC, tube-type IEC, and heat-pipe-based IEC are mainly studied with different airflow directions, such as in parallel flow, counter flow, and cross flow [4-6]. As shown in Fig. 1, two separate airstreams namely the primary (product) air and secondary (working) air, flow along dry channels and wet channels from horizontal and vertical entrances, respectively. The spraying water on the surfaces of the wet channels is circulated from the water tank to the top-hanging nozzles by a pump. Driven by moisture content difference, the spraying water evaporates when the air passes the wet channels, which removes the heat from the plate. Therefore, the air in the dry channel is cooled by the plate through the convective heat transfer.

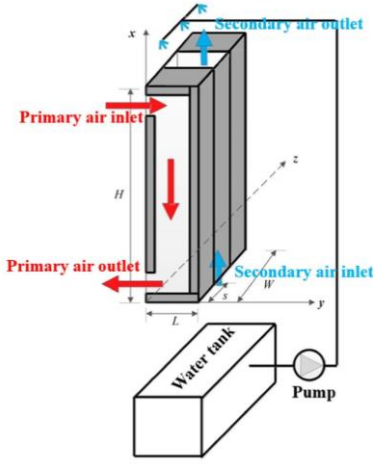

Fig. 1 Schematic diagram of the counterflow IEC [5]

II. LITERATURE REVIEW

In general, the enhanced measures for the cooling performance of IEC have been proposed from many perspectives. Firstly, the dew point IEC, represented by M-cycle cooler and regenerative IEC (RIEC), was proposed to break through the limit of outlet air temperature. A proportion of the processed air at low wet-bulb temperature was introduced to the wet channel. For instance, Zhan et al. conducted a comparative study between conventional IEC and M-cycle IEC in the same physical geometry. The latter one was proved to supply the air with lower temperature than the former one. The wet-bulb efficiency of the dew point IEC was more than 100% in some cases, especially in hot and arid regions. [7, 8]. In addition to extracting the cool air to the wet channel, several novel internal structures were also reported to enhance the performance. Corrugated wicks were embedded into the wet channel to increase the contact area of spraying water [9]. Internal baffles were added in the dry channel by Kabeel et al. to generate small local vortexes, consequently, improved the convective heat transfer rate [10]. Results indicated that the supply air temperature reduced from 15.1% to 20.5% when the number of baffles varied from 9 to 15.

Apart from the two methods above, the cooling performance enhancement of IEC can be achieved by improving the surface wettability, which currently includes attaching water-absorbent materials and covering the hydrophilic coating. Materials such as felt, fabric, cotton, Kraft paper, and nylon fiber have been used in the wet channel of IEC, and were proven to be able to retain more water than the smooth surface. [10-13]. However, the wetted fiber was pointed out the weak antibacterial ability, causing the extra cost of operating maintenance [14]. With respect to the coating, Guilizzoni et al. evaluated the contact angle and water retention ability of the surfaces covering standard epoxy coating (STD) and hydrophilic lacquer (HPHI) [15]. Experimental results showed that the HPHI could exert a lower contact angle than STD, which therefore enhances the hydrophilicity in the secondary air channel and achieves 10% cooling capacity enhancement.

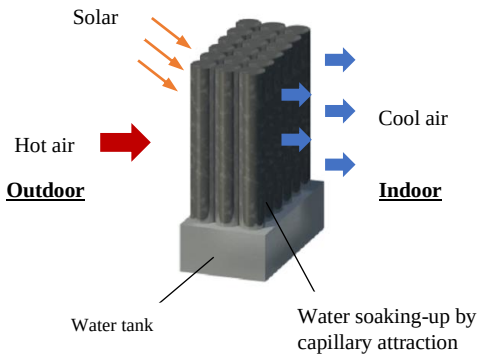

(a) DEC [16]

(b) Tubular porous ceramic IEC [17]

Fig. 2 Passive evaporative cooling using porous materials

As for the application of porous media, Chen et al. analyzed the cooling potential of a cooler with heat exchanger walls made of porous ceramic pipes. As shown in Fig. 2(a), the porous pipes were placed in a water tank to absorb the water for evaporation. Due to the capillary action, the water could be sucked on the surface of the pipe. The evaporation happened when the air was passing through the pipe so as to remove the sensible cooling load. From the experimental results, up to 5℃ temperature drop would be achieved [16]. Regarding the IEC with porous media, the existing literature is still limited compared with the normal IEC. Studies that investigated the characteristics of IEC using porous media are summarized as follows. Referring to Lee and Lee, porous layer coating was covered in the finned wet channels of a RIEC to enhance the surface wettability [18]. The porous fiber was employed on the surface of secondary air passages for the same purpose [19]. Riffat and Zhu proposed a heat-pipe-based IEC with a ceramic water container in an early study [20]. This study was continued by Amer with sufficient theoretical and experimental works [21]. Results showed that the maximum temperature drop and COP contributed by the IEC were 17.1℃ and 17.02, respectively. Besides, the air with inlet temperature below 42℃ and relative humidity (RH) less than 30% can be conditioned into the human comfort zone by the cooler. The potential and feasibility of the IEC made of porous clay pipes were evaluated under subtropical weather conditions [22]. The pipes in staggered and aligned arrangements were also analyzed for performance optimization. Wang et al. conducted experiments for a tube-type porous ceramic IEC (Fig. 2(b)), realizing the intermittent spraying strategy of the water system [17]. Results revealed that the cool air can be produced smoothly for 100 minutes after thoroughly wetted by spraying water. Recently, Sun et al. [23, 24] conducted a theoretical analysis of tube-type porous ceramic IEC and optimized the pipe spacing, tube length, nozzle type, and spraying strategies.

Based on the existing literature, it is noticed that the porous media has been employed in DEC and tubular IEC. However, the plate-type IEC with the porous media surface on the secondary air channel is yet to be investigated, let alone the time-independent dynamic performance prediction, which motivates this study. The model establishment and preliminary results are presented in the following sections.

III. MODEL ESTABLISHMENT

In this section, the plate-type counterflow IEC model with porous media on the secondary air surface (PIEC) is built. The symmetric unit of the physical model consists of half of a primary channel and half of a secondary air channel, referring to Fig. 3. The main assumptions used for establishing the heat and mass transfer equations are listed as follows.

1) The water film and air are considered steady and incompressible in two channels.
2) The flow status in both the free zone and the porous zone is regarded as the laminar flow.
3) There is no heat and mass exchange between the IEC and surroundings.

4) The water pump is turned off when the moist porous media is fully wetted. Evaporation only occurs in the porous media full of water.
5) The water that leaves from the porous zone is in the form of vapor.
6) The air velocity is constant, and it only depends on the inlet setting conditions.
7) The pores have direct contact with the working air, and are evenly distributed in similar geometric sizes with no closed air cavity.

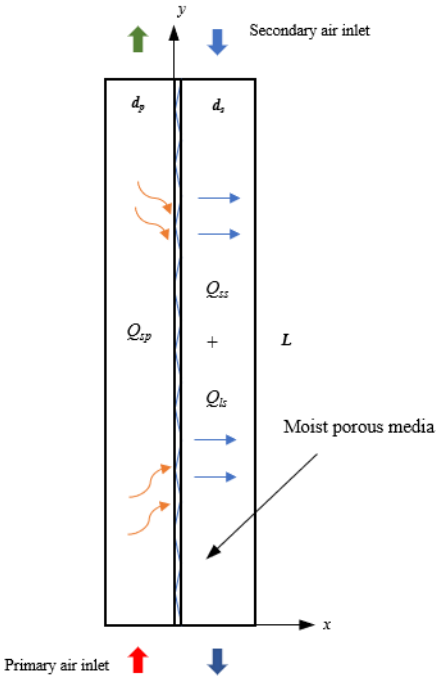

Fig. 3 Modeling of the counterflow PIEC

A. *Free zone*

The physical model of IEC contains two free zones and a porous zone. Free zones are full of moist air, while the porous zone includes moist air and liquid water. Regarding the free zone that includes primary air and secondary air, the continuity equation, momentum conservation equation, energy equation, and species diffusion with the time-independent item are written in Eq.(1) - Eq. (5).

$$\frac{\partial u_i}{\partial x}+\frac{\partial v_i}{\partial y}=0 \tag{1}$$

$$\frac{\partial u_i}{\partial \tau}-\frac{1}{\rho}\frac{\partial P_i}{\partial x}+\frac{\mu}{\rho}\left(\frac{\partial^2 u_i}{\partial x^2}+\frac{\partial^2 u_i}{\partial y^2}\right)-\left(u_i\frac{\partial u_i}{\partial x}+v_i\frac{\partial v_i}{\partial y}\right)=0 \tag{2}$$

$$\frac{\partial v_i}{\partial \tau}-\frac{1}{\rho}\frac{\partial P_i}{\partial y}+\frac{\mu}{\rho}\left(\frac{\partial^2 v_i}{\partial x^2}+\frac{\partial^2 v_i}{\partial y^2}\right)-\left(u_i\frac{\partial u_i}{\partial x}+v_i\frac{\partial v_i}{\partial y}\right)=0 \tag{3}$$

$$\rho_g C_{pg}\left(\frac{\partial t_i}{\partial \tau}+u_i\frac{\partial T_i}{\partial x}+v_i\frac{\partial T_i}{\partial y}\right)=k_g\left(\frac{\partial^2 t_i}{\partial x^2}+\frac{\partial^2 t_i}{\partial y^2}\right) \tag{4}$$

$$\frac{\partial c_s}{\partial \tau}+u_s\frac{\partial c_s}{\partial x}+v_s\frac{\partial c_s}{\partial y}=D_{va}\left(\frac{\partial^2 c_s}{\partial x^2}+\frac{\partial^2 c_s}{\partial y^2}\right) \tag{5}$$

where i = p, s

The relationship between saturation pressure and temperature is given by Eq. (6) and Eq.(7) [25].

$$\ln(P_{q_b})=\frac{a_1}{T_w}+a_2+a_3T_w+a_4T_w^2+a_5T_w^3+a_6\ln(T_w) \tag{6}$$

$$c_{sat}=\frac{0.622P_{qb}}{B-P_{qb}} \tag{7}$$

where: a_1 = -5800.2206, a_2 = 1.3914993, a_3 = -0.04860239, a_4 = $-4.1764769105\times10^{-5}$, a_5 = -1.4452093×10^{-8}, a_6 = 6.5459673, B = 101.325 kPa

The mass transfer and energy balance of the wet porous media interface and secondary air are discussed in part B of this section.

B. *Porous zone*

For the porous region, the water and gas saturation, which describe the content of the water and moist air in the porous media, are presented in Eq. (8) [26]. The effective thermal conductivity and specific heat capacity of the porous media, that alter the conductivity of liquid phase and porosity, are modified using Eq. (9) and Eq. (10).

$$S_w+S_g=1 \tag{8}$$

$$k_{eff}=k_s(1\text{-}\varepsilon)+k_wS_w\varepsilon+k_gS_g\varepsilon \tag{9}$$

$$(\rho c_p)_{eff}=\rho_s c_{ps}(1\text{-}\varepsilon)+\rho_w c_{pw}S_w\varepsilon+\rho_g c_{pg}S_g\varepsilon \tag{10}$$

In the porous zone, the velocity and pressure distribution of water and moist air can be calculated using Darcy's law and the Brinkman equation, shown in Eq. (11) and Eq. (14).

$$\boldsymbol{u_l}=-\frac{\kappa\kappa_{rl}}{S_l\mu_l\varepsilon}\nabla P_l \tag{11}$$

$$S_l=\frac{c_wM_w}{\rho_w\varepsilon} \tag{12}$$

$$P_l=P_g-P_c \tag{13}$$

$$\nabla P_g=-\frac{\mu_g}{\kappa\kappa_{rg}}\boldsymbol{u_g}+\mu_g\nabla^2\boldsymbol{u_g} \tag{14}$$

$$\nabla\cdot\boldsymbol{u_g}=0 \tag{15}$$

The liquid phase permeability depends on the absolute permeability and relative liquid permeability. Also, the gas phase permeability follows a similar rules, as expressed in Eq. (16) and Eq. (17). The absolute permeability is obtained by Carman-Kozeny shown as Eq. (18), which depends on the porosity and pore diameter [27]. Meanwhile, the relative permeabilities of the gas phase and liquid phase are given by Eq. (19)-(20) [26, 28].

$$\kappa_g=\kappa\kappa_{rg} \tag{16}$$

$$\kappa_w=\kappa\kappa_{rw} \tag{17}$$

$$\kappa=\frac{d_{por}^2}{180}\cdot\frac{\varepsilon^3}{(1-\varepsilon)^2} \tag{18}$$

$$\kappa_{rg}=1-1.1S_l,\quad \left(S_l<\frac{1}{1.1}\right) \tag{19}$$

$$\kappa_{rw}=\left(\frac{S_l-S_{lr}}{1-S_{lr}}\right)^3,\quad (S_l>S_{lr}) \tag{20}$$

The liquid water is assumed to leave the porous media in the form of vapor, taking away the latent heat simultaneously. The increase of moisture content in the secondary air equals the reduced liquid water content in the porous region. In addition, the porous structure could lead to the capillary action, which is usually regarded as an extra diffusion item in the mass transfer process [26]. Considering the above physical behaviors, the mass transfer and the energy equilibrium during the evaporation process are given in Eq. (21) to Eq. (23). The diffusivity of the moist air in the porous region is influenced by the gas saturation and porosity, so the effective diffusivity is modified using Eq. (24) [29-31]. The water diffusion caused by capillary action is determined by the temperature and water vapor content, as expressed in Eq. (25).

$$\frac{\partial \rho_g S_g \varepsilon}{\partial \tau} + \left(-\frac{\rho_g D_{va\_eff}}{1-c}\frac{\partial c_s}{\partial x}\right) = m \quad (21)$$

$$\frac{\partial c_w}{\partial \tau} + \left(-D_{cap}\frac{\partial^2 c_w}{\partial y^2}\right) + u_w\frac{\partial c_w}{\partial x} + v_w\frac{\partial c_w}{\partial y} = -m \quad (22)$$

$$Q_{p,senible} = Q_{s,senible} + m \cdot h_{fg} \quad (23)$$

$$D_{va\_eff} = D_{va}(S_g\varepsilon)^{\frac{4}{3}} \quad (24)$$

$$D_{cap} = 2.8945e^{\left(1.26X_m - 2.76{X_m}^2 + 4.96{X_m}^3 - \frac{6117.4}{T}\right)} \quad (25)$$

C. *Numerical solutions*

The governing equations mentioned above were numerically solved using COMSOL Multiphysics software. The heat transfer module, laminar flow module, transport of diluted species module, and some self-defined equations were incorporated according to the above description. The velocities of air in two channels only depend on the inlet setting conditions and could not vary with time, which was treated as steady status in the calculation process. Boundary conditions were summarized and set to the model. The initial values are set as the inlet air conditions in the dry and wet channels, and the porous zone initial temperature is decided by the spraying water with normal temperature from the building water supply system. In order to enhance the cooling performance, the return air from the indoor air-conditioned spaces was employed as the secondary air. Due to the lower wet-bulb temperature, the outlet primary air can be greatly reduced compared with the case using 100% outdoor fresh air. Essential parameters for simulations are presented in Table 1. Multifrontal Massively Parallel sparse direct Solver (MUMPS), which is useful in solving the sets of equations generated by the finite element method, was employed to calculate the aimed distributions for each element. The whole solving process for the temperature field, humidity field, and velocity field was illustrated in Fig 4. The parameters related to the porous media in IEC were provided by the specialized porous material manufacturer.

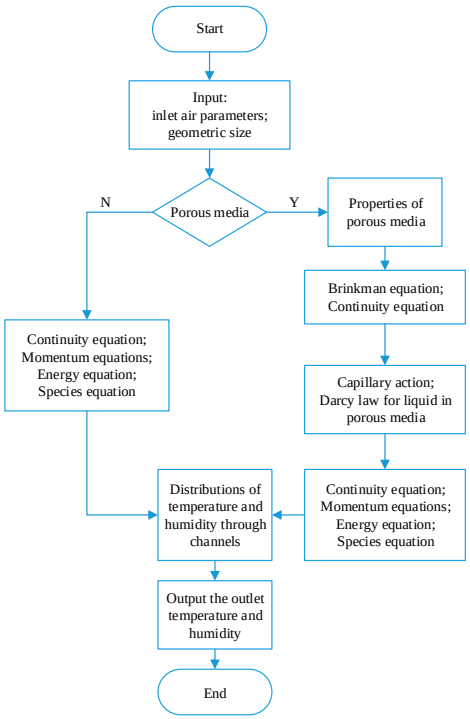

Fig. 4 The flow chart for the solving process for PIEC

Table 1 The pre-set values for simulations

Parameter	Value	Parameter	Value
H (mm)	400	Tp_i (℃)	30
d (mm)	4	RHp_i	0.4
$d_{\_por}$ (mm)	0.1	Ts_i (℃)	24
ε	0.8	RHp_s	0.5
h_{fg} (J/kg)	2.5×10^{6}	Tw_i (℃)	22
D_va (m^2/s)	2.6×10^{-5}	v_p (m/s)	2
S_ir	0.1	v_s (m/s)	2
Total time (s)	1000	Time interval (s)	5

Note: S_ir is the irreducible liquid phase saturation, representing the water that stays in the porous media and unable to be evaporated. The normal value of S_ir is around 0.1, and which has been commonly adopted in the published literature [26].

IV. RESULTS AND DISCUSSIONS

Based on the input parameters, the temperature and humidity distributions in the PIEC were obtained, as presented in Fig 5. The primary air was cooled along the left channel, which entered at 30℃ and exhausted with a 9.3℃ temperature drop on average. The moisture content of primary air remained constant at 0.0106 kg/kg in the dry channel. In the wet channel, the air state started from 0.0093 kg/kg at the entrance and changed to 0.0162 kg/kg when it escaped the channel.

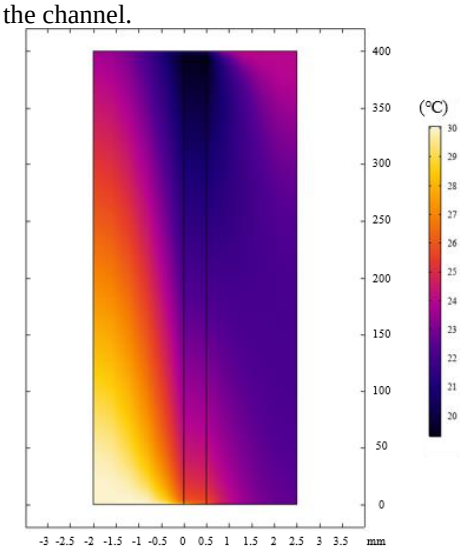

(a) Temperature

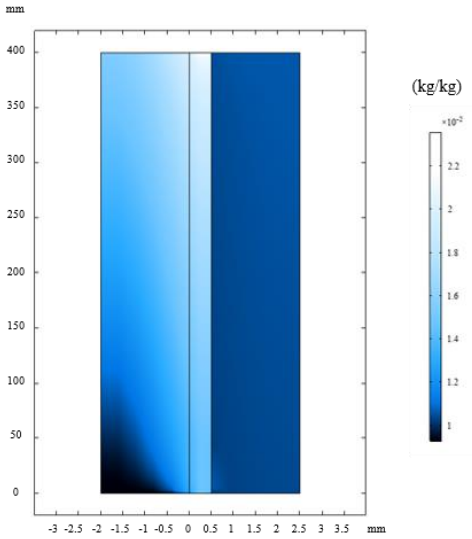

(b) Moisture content

Fig. 5 Distributions of (a) temperature (b) moisture content in the PIEC at 500s

In addition, the variation of primary air temperature at outlet was also simulated within the first 500 seconds, as presented in Fig 6. The secondary air promoted the evaporation in the wet channels, taking away the latent heat and causing the temperature reduction. The outlet primary air temperature decreased significantly to 21.4℃ in the first 50 seconds. After that, the outlet temperature slightly reduced by 0.5℃ from 100 seconds to 500 seconds, which meant that the water was temporarily sufficient for supporting the evaporation in the moist porous media during the calculation period.

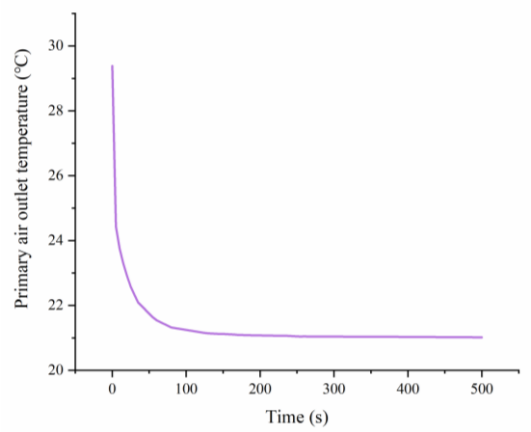

Fig. 6 The variation of the primary air outlet temperature during the first 500s

Table 2 The pre-set values for simulations

Parameter	Value
d_por (mm)	[0.01, 0.01, 0.1] [0.1, 0.1, 0.5]
ε	[0.5, 0.1, 0.9]
Time interval (s)	5
Total time (s)	2000

Note: [a, b, c]: starts from a and ends at b with c interval.

A. *Effect of the porosity*

As shown in Fig. 7, the cooling limit of PIEC could decrease with the increase of the porosity. The lowest temperature was 22.4℃ when the porosity was 0.5, while it decreased to 21℃ when the porosity increased to 0.9. Furthermore, it was observed that the transition point from temperature drop to temperature rise delayed against the porosity enlargement. Specifically, the temperature began to slightly rise after 420 seconds in the 0.5 porosity case, but it started to go up since 820 seconds in the 0.9 porosity case.

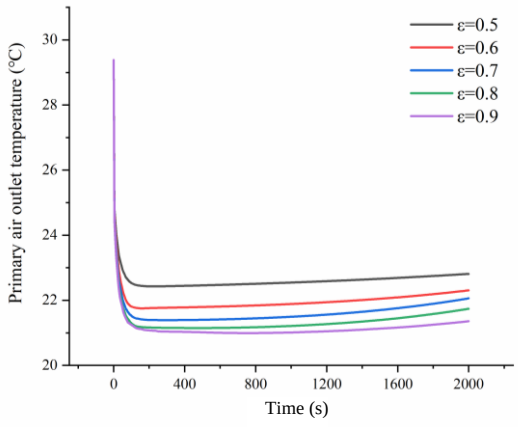

Fig. 7 The effect of the porosity on the primary air outlet temperature in the first 2000 seconds

The main reasons for the tendency of cooling performance were illustrated as follows. Firstly, the large porosity led to a greater evaporation rate, thus removed more latent heat in the wet channel [32]. Secondly, the higher porosity improved the water retention ability. Therefore, more water could be stored for an extended evaporation period.

B. *Effect of the pore diameter*

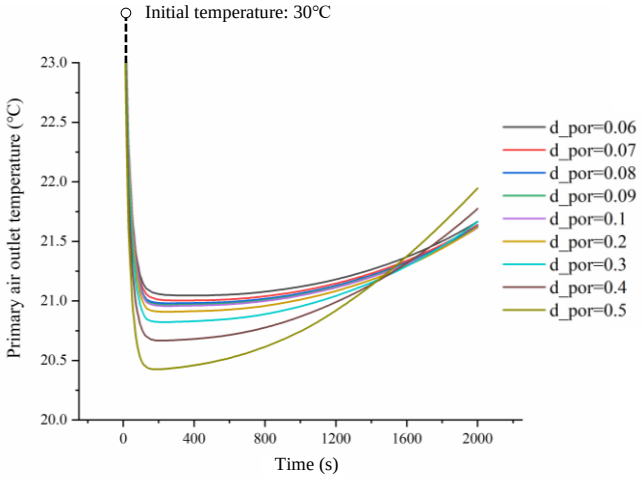

Fig. 8 The effect of the pore diameter on the primary air outlet temperature in the first 2000 seconds

As described in Fig. 8, when the pore diameter was less than 0.1mm, the duration for maintaining the stable outlet temperature was almost the same, and the product air temperature was around 21℃. Meanwhile, a lower temperature was obtained with the growth of pore diameter at the cost of a shorter stable duration, especially when the value was over 0.2mm. The reason for this series of tendencies was given: the larger pore was proved to promote evaporation and shorten the evaporation period in other industries [33]. Nonetheless, the enhanced cooling effect was closely related to the specific pore size.

V. CONCLUSION

This study established a counter flow PIEC model with time-independent cooling performance prediction. The cool indoor air was utilized as the source of the secondary air. The effects of the porous media parameters on the cooling performance were presented, namely, the porosity and pore diameter. The main conclusions are listed as follows.

1) The larger porosity and pore diameter contributed to a higher evaporation rate, thus a lower outlet primary air temperature could be obtained. The enhanced perfomance faded with the increase of the porosity value. Nonetheless, it became more prominent with the growing pore diameter.

2) The higher porosity means a longer stable evaporation duration after turning off the pump. Increasing the pore diameter had little influence on the duration, but the effect was intensified if the pore diameter exceeds a certain value.

3) Porous media was expected to absorb and retain more water, which potentially enables the water spraying module in the PIEC system to operate intermittently. The results of this study predicted temperature variation tendencies in the PIEC, which was beneficial for designing the periodically

control strategy, eventually saving electrical energy and water resources.

ACKNOWLEDGMENT

The authors wish to acknowledge the financial support provided by the General Research Fund projects of the Hong Kong Research Grant Council (Ref. No.: 15213219 and 15200420).

REFERENCES

[1] Wu T, Cao B, Zhu Y. A field study on thermal comfort and air-conditioning energy use in an office building in Guangzhou. Energy and buildings. 2018;168:428-37.
[2] Hong Kong Energy End-use Data 2020. Hong Kong, (EMSD) TEaMSD; 2020.
[3] Duan Z, Zhan C, Zhang X, Mustafa M, Zhao X, Alimohammadisagvand B, et al. Indirect evaporative cooling: Past, present and future potentials. Renewable and Sustainable Energy Reviews. 2012;16(9):6823-50.
[4] Chen Y, Yang H, Luo Y. Indirect evaporative cooler considering condensation from primary air: Model development and parameter analysis. Building and Environment. 2016;95:330-45.
[5] Min Y, Chen Y, Yang H. Numerical study on indirect evaporative coolers considering condensation: A thorough comparison between cross flow and counter flow. International Journal of Heat and Mass Transfer. 2019;131:472-86.
[6] Cui X, Chua KJ, Yang WM. Numerical simulation of a novel energy-efficient dew-point evaporative air cooler. Applied Energy. 2014;136:979-88.
[7] Rogdakis ED, Koronaki IP, Tertipis DN. Experimental and computational evaluation of a Maisotsenko evaporative cooler at Greek climate. Energy and Buildings. 2014;70:497-506.
[8] Riangvilaikul B, Kumar S. Numerical study of a novel dew point evaporative cooling system. Energy and Buildings. 2010;42(11):2241-50.
[9] Park J-Y, Kim B-J, Yoon S-Y, Byon Y-S, Jeong J-W. Experimental analysis of dehumidification performance of an evaporative cooling-assisted internally cooled liquid desiccant dehumidifier. Applied Energy. 2019;235:177-85.
[10] Kabeel AE, Abdelgaied M. Numerical and experimental investigation of a novel configuration of indirect evaporative cooler with internal baffles. Energy Conversion and Management. 2016;126:526-36.
[11] Golizadeh Akhlaghi Y, Badiei A, Zhao X, Aslansefat K, Xiao X, Shittu S, et al. A constraint multi-objective evolutionary optimization of a state-of-the-art dew point cooler using digital twins. Energy Conversion and Management. 2020;211.
[12] Chen Y, Luo Y, Yang H. Fresh Air Pre-cooling and Energy Recovery by Using Indirect Evaporative Cooling in Hot and Humid Region – A Case Study in Hong Kong. Energy Procedia. 2014;61:126-30.
[13] Khalid O, Ali M, Sheikh NA, Ali HM, Shehryar M. Experimental analysis of an improved Maisotsenko cycle design under low velocity conditions. Applied Thermal Engineering. 2016;95:288-95.
[14] Zhao X, Liu S, Riffat SB. Comparative study of heat and mass exchanging materials for indirect evaporative cooling systems. Building and Environment. 2008;43(11):1902-11.
[15] Guilizzoni M, Milani S, Liberati P, De Antonellis S. Effect of plates coating on performance of an indirect evaporative cooling system. International Journal of Refrigeration. 2019;104:367-75.
[16] Chen W, Zhang S, Zhang Y. Analysis on the cooling and soaking-up performance of wet porous wall for building. Renewable Energy. 2018;115:1249-59.
[17] Wang F, Sun T, Huang X, Chen Y, Yang H. Experimental research on a novel porous ceramic tube type indirect evaporative cooler. Applied Thermal Engineering. 2017;125:1191-9.
[18] Lee J, Lee D-Y. Experimental study of a counter flow regenerative evaporative cooler with finned channels. International Journal of Heat and Mass Transfer. 2013;65:173-9.
[19] Duan Z, Zhan C, Zhao X, Dong X. Experimental study of a counterflow regenerative evaporative cooler. Building and Environment. 2016;104:47-58.
[20] Riffat SB, Zhu J. Mathematical model of indirect evaporative cooler using porous ceramic and heat pipe. Applied Thermal Engineering. 2004;24(4):457-70.
[21] Amer O. A heat pipe and porous ceramic based subwet-bulb temperature evaporative cooler: University of Nottingham; 2017.
[22] Ramkumar R, Ragupathy A. Experimental investigation of indirect evaporative cooler using clay pipe. Journal of Thermal Engineering. 2017;3(2):1163-80.
[23] Sun T, Huang X, Qu Y, Wang F, Chen Y. Theoretical and experimental study on heat and mass transfer of a porous ceramic tube type indirect evaporative cooler. Applied Thermal Engineering. 2020;173.
[24] Sun T, Huang X, Chen Y, Zhang H. Experimental investigation of water spraying in an indirect evaporative cooler from nozzle type and spray strategy perspectives. Energy and Buildings. 2020;214.
[25] ASHRAE. ASHRAE Handbook of Fundamentals: Mar Lin Book Company; 1985.
[26] Su T, Zhang Z, Han J, Zhang S, Wang X, Zhang W. Sensitivity analysis of intermittent microwave convective drying based on multiphase porous media models. International Journal of Thermal Sciences. 2020;153.
[27] Kaviany M. Principles of heat transfer in porous media. 2nd ed.. ed. New York: Springer-Verlag Inc.; 1995.
[28] Liu W. Theory and application of heat and mass transfer in porous media. First edition ed. Fan A, Huang X, editors. Beijing: Beijing: Science Press; 2006.
[29] Datta AK. Porous media approaches to studying simultaneous heat and mass transfer in food processes. II: Property data and representative results. Journal of Food Engineering. 2007;80(1):96-110.
[30] Purlis E. Modelling convective drying of foods: A multiphase porous media model considering heat of sorption. Journal of Food Engineering. 2019;263:132-46.
[31] Kumar C, Joardder MUH, Farrell TW, Karim MA. Multiphase porous media model for intermittent microwave convective drying (IMCD) of food. International Journal of Thermal Sciences. 2016;104:304-14.
[32] LI Hongru CY, ZHANG Jingcao, XIN Gongming. Evaporation in porous media with different porosity. CIESC Journal. 2017;68(9):3380-7.
[33] Aboufoul M, Shokri N, Saleh E, Tuck C, Garcia A. Dynamics of water evaporation from porous asphalt. Construction and Building Materials. 2019;202:406-14.